

Effects of tropical North Atlantic sea surface temperature on intense tropical cyclones landfalling in China

Si Gao^{1,2} | Zhifan Chen³ | Wei Zhang⁴  | Xinyong Shen^{3,2}

¹School of Atmospheric Sciences, and Guangdong Province Key Laboratory for Climate Change and Natural Disaster Studies, Sun Yat-sen University, Zhuhai, China

²Southern Marine Science and Engineering Guangdong Laboratory (Zhuhai), Zhuhai, China

³Key Laboratory of Meteorological Disaster, Ministry of Education, and Collaborative Innovation Center on Forecast and Evaluation of Meteorological Disaster, Nanjing University of Information Science and Technology, Nanjing, China

⁴IIHR-Hydroscience & Engineering, The University of Iowa, Iowa City, Iowa, USA

Correspondence

Wei Zhang, IIHR-Hydroscience & Engineering, The University of Iowa, Iowa City, IA.

Email: wei-zhang-3@uiowa.edu

Funding information

National Key R&D Program of China, Grant/Award Number: 2019YFC1510400; National Natural Science Foundation of China, Grant/Award Numbers: 41930967, 41575078, 41975054; Strategic Priority Research Program of the Chinese Academy of Science, Grant/Award Number: XDA20100304

Abstract

This study identifies a significant positive association between tropical North Atlantic (TNA) sea surface temperature (SST) during preceding spring and the frequency of intense tropical cyclones (TCs) making landfall over mainland China during autumn on interannual time scales. Observational analyses show that a warm SST anomaly in TNA during spring can induce a warm SST anomaly in the western part of the western North Pacific (WNP) in subsequent autumn, through a chain of air-sea coupled processes such as Rossby-wave response, wind-evaporation-SST feedback, and westward advection of warm surface water. The physical mechanisms are verified using a suite of coupled numerical experiments performed by the state-of-the-art Community Earth System Model. The warm SST anomaly in the western part of WNP is responsible for the genesis and intensification of intense TCs in situ, and the climatologically mean southeasterly steering flow is favourable for the intense TCs to make landfall over mainland China.

KEYWORDS

China, coupled numerical experiments, intense tropical cyclone landfall, interannual variation, tropical North Atlantic SST

1 | INTRODUCTION

Landfalling tropical cyclones (TCs) are among the most destructive natural phenomena in highly-urbanized coastal regions by leading to torrential rains, flooding, strong winds, and storm surges (Mendelsohn *et al.*, 2012; Zhang *et al.*, 2018a), and this is particularly true for mainland China that is subjected to havoc caused by landfalling TCs. For example, Super Typhoon Herb, which made landfall in Fujian Province in 1996, resulted

in economic losses of 73.2 billion yuans and killed 779 people; Super Typhoon Fred, which made landfall in Zhejiang Province in 1994, was responsible for 1,126 fatalities and 24-billion-yuan economic losses (Zhang *et al.*, 2009). Thus, a better understanding of the variability in landfalling intense TCs in China is of great scientific interest and profound socioeconomic significance.

Previous studies have investigated the trends in landfalling TCs in China. For example, an abrupt change in TC occurrence around Taiwan in 2000 was attributed

to a northward shift of TC track associated with warm sea surface temperature (SST) anomaly (SSTA) in the western and central equatorial Pacific (Tu *et al.*, 2009). Consistent increasing trends in frequency and/or intensity of landfalling TCs in East China were found (Wu *et al.*, 2005; Park *et al.*, 2014; Li *et al.*, 2017). However, the reported trends in landfalling TC activity in South China were divergent. Some studies (Zhang *et al.*, 2012b; Li *et al.*, 2017; Zhang *et al.*, 2019) showed no significant trend in landfalling TC intensity or frequency in South China. Park *et al.* (2014) suggested no trend in landing TC frequency but a downward trend in landfalling TC intensity in South China. Mei and Xie (2016) found upward trend in landing TC intensity in South China. In addition, Lok and Chan (2017) projected fewer but stronger TCs landfalling in South China in the late 21st century.

Interannual variation of landing TCs in China has also been extensively examined. There is a negative correlation between landfalling TC frequency in China with the El Niño–Southern Oscillation (ENSO). More (Less) TCs make landfall in South China during La Niña (El Niño) years, resulting from the changes in genesis location and steering flow associated with anomalous large-scale circulation (Elsner and Liu, 2003; Liu and Chan, 2003; Wu *et al.*, 2004; Zhang *et al.*, 2012a; Zhang *et al.*, 2016). Liu and Chan (2018) further showed that the relationship between La Niña and TC landfalls in South China changed in 1997, possibly due to the changes in genesis frequency and location as well as track pattern associated with the changes in large-scale circulations. Fogarty *et al.* (2006) identified a dipole pattern of TC landfalls in southern and northern provinces and related it to northwestern Pacific SST and the difference in sea level pressure between western China and Mongolia. The SST gradient between the tropical Indian Ocean and the western Pacific warm pool in boreal spring has a significant negative impact on summer TC landfalls in China (Wang and Chen, 2018a). The onset date of South China Sea summer monsoon also shows a significant negative correlation with TC landfalls in China in peak TC season (Wang and Chen, 2018b). Most recently, Gao *et al.* (2020) found a significant impact of the Pacific Meridional Mode on TC landfalls in China.

Given significant impacts of tropical North Atlantic (TNA) SST on the western North Pacific (WNP) TC frequency (Huo *et al.*, 2015; Cao *et al.*, 2016; Yu *et al.*, 2016; Zhang *et al.*, 2018b) and on landfalling TC frequency over all the countries in East Asia except for the Philippines (Gao *et al.*, 2018a), one may expect that TNA SST also exerts a negative effect on the frequency of intense TCs landfalling in a certain country/region in East Asia. The objective of this study is thus to examine whether, the extent to which and how TNA SST affects the frequency

of intense TCs landfalling in China on interannual time scales, through observational data analysis and numerical experiments. Section 2 describes data and methods, results are presented in Section 3, and Section 4 includes summary and discussion.

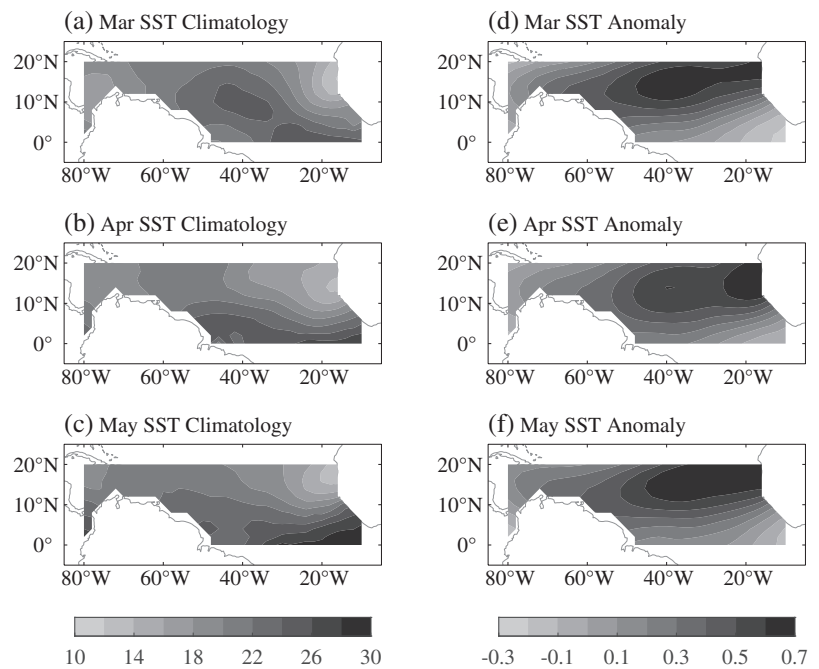
2 | DATA AND METHODS

The study period of this paper is 1979–2017. We use the Joint Typhoon Warning Center (JTWC) TC best-track data set, which better archives TC intensity than the other best-track data sets (Chan, 2008; Wu and Zhao, 2012). An intense TC is defined as a category 4–5 TC (maximum 1-min sustained wind speed $\geq 58 \text{ m}\cdot\text{s}^{-1}$) on the Saffir-Simpson Scale, following previous studies (e.g., Chan, 2007, 2008; Zhang *et al.*, 2015; Gao *et al.*, 2018b). A detection algorithm (see details in Gao *et al.*, 2018a) is used to identify the frequency of intense TCs landfalling in mainland China. TC genesis is defined as occurring when a TC first reaches the tropical storm strength (i.e., maximum sustained wind $\geq 17 \text{ m}\cdot\text{s}^{-1}$). Rapid intensification is defined as 24-hr intensity change (ΔV_{24}) $\geq 15 \text{ m}\cdot\text{s}^{-1}$, slow intensification is defined as $0 \text{ m}\cdot\text{s}^{-1} < \Delta V_{24} < 15 \text{ m}\cdot\text{s}^{-1}$, and decay is defined as $\Delta V_{24} \leq 0 \text{ m}\cdot\text{s}^{-1}$, following Gao *et al.* (2016, 2017).

Monthly atmospheric variables with $2.5^\circ \times 2.5^\circ$ resolution are obtained from the National Center for Environmental Prediction (NCEP)/National Center for Atmospheric Research (NCAR) reanalysis product (Kalnay *et al.*, 1996). Monthly precipitation data with $2.5^\circ \times 2.5^\circ$ resolution are attained from the Global Precipitation Climatology Project (GPCP) analysis product version 2.3 (Adler *et al.*, 2018). Monthly SST data with $2^\circ \times 2^\circ$ resolution are acquired from the National Oceanic and Atmospheric Administration (NOAA) Extended Reconstructed Sea Surface Temperature (ERSST) version 4 (Huang *et al.*, 2015). These oceanic and atmospheric variables are detrended first to only examine the interannual variabilities.

Coupled perturbation experiments are performed to verify the mechanisms governing the effect of spring (March–May, MAM) TNA SST on large-scale circulation during subsequent autumn (September–November, SON), using version 1.2 of the NCAR Community Earth System Model (CESM, Hurrell *et al.*, 2013) with T31_gx3v7 horizontal resolution ($\sim 3.75^\circ \times 3.75^\circ$ resolution for atmosphere and nominal 3° resolution for ocean). This climate model has 26 vertical levels for atmosphere and 60 vertical levels for ocean. We perform two experiments: one is prescribed with the monthly SST climatology during our study period 1979–2017 (CTRL experiment), and the other with the average monthly SST

FIGURE 1 The prescribed SST climatology in (a) March, (b) April, and (c) May for the CTRL experiment and the prescribed SST anomaly in (d) March, (e) April, and (f) May for the TNA experiment



anomaly during six warm TNA SST years (see Section 3) adding to the monthly SST climatology (TNA experiment). The restoring of SST climatology and anomaly in the CTRL and TNA experiments are only conducted in TNA (0° – 20° N, 80° – 10° W) for each month of MAM (Figure 1), whereas the model is fully coupled over the other regions and during the other periods. The fixed pre-industrial radiative forcing is used in the two experiments. The CESM spins up for 199 years and is integrated for additional 5 years. We set five ensemble members by using the resulting fields from the additional 5-year integration as initial conditions, and then each ensemble member is integrated for 15 years. To avoid initial shock (e.g., Chen *et al.*, 1995), we compare the ensemble-mean differences between the TNA and CTRL experiments during the last 10 years, which represent the forced responses to the warm TNA SSTA during MAM.

3 | RESULTS

Figure 2 indicates the normalized time series of the Niño 3.4 index in preceding winter (December–February, DJF) and detrended TNA (0° – 20° N, 80° – 10° W) SSTA in MAM without ENSO signal (the linear regression onto Niño 3.4 index in preceding winter is subtracted) as well as the time series of frequency of intense TCs landfalling in mainland China in SON during the study period. The

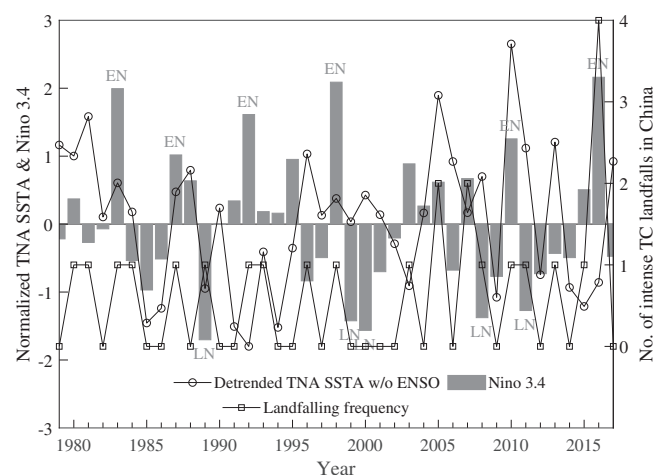


FIGURE 2 Time series of the frequency of intense TCs landfalling in mainland China during SON (line with squares) and normalized time series of Niño 3.4 index during preceding DJF (grey bar) and detrended TNA SSTA during MAM without ENSO signal (line with circles). EN and LN denote typical El Niño and La Niña years, respectively

mean SON frequency of intense TCs landfalling in mainland China is 0.6, although it is a small number, it represents one third of the mean SON frequency of all TCs landfalling in mainland China (i.e., 1.8) and each landfall of intense TCs can cause tremendous damage. Based on

one standard deviations of the above SST indices, six warm TNA SST years (1979, 1980, 1981, 1996, 2005, and 2013) and six cold TNA SST years (1985, 1986, 1991, 1994, 2009, and 2015) are selected after excluding 11 typical ENSO events (El Niño years: 1983, 1987, 1992, 1998, 2010, and 2016; La Niña years: 1989, 1999, 2000, 2008, and 2011), due to the close association of intense TC landfalls in mainland China during SON with the ENSO signal during preceding winter (their correlation is 0.48, $p < .01$). During the remaining 29 neutral-ENSO years, SON frequency of intense TCs landfalling in mainland China has a correlation of 0.39 with MAM TNA SSTA, their partial correlation is 0.41 if further controlling the Niño 3.4 index in preceding DJF. Both correlations are significant above the 95% confidence level, suggesting a strong association of MAM TNA SSTA with the SON frequency of intense TCs landfalling in mainland China, which is independent of ENSO effects. This seasonal lag chain between TNA SSTA in MAM and landfalling TCs in China in SON is unique, since we do not find any other significant correlations of intense TC landfalls in China with TNA SSTA in other seasons.

Figure 3 shows the tracks of all intense TCs during SON of selected warm and cold TNA SST years as well as their difference in genesis density. There are 22 and 24 intense TCs during SON of six warm and six cold TNA SST years, respectively. Intense TCs tend to generate in the western part of the WNP (WWNP) and six of them make landfall in mainland China during SON of warm TNA SST years, while intense TCs tend to form over the southeastern part of the WNP and only one of them make landfall in mainland China during SON of cold TNA SST years. The mean frequency of intense TCs landfalling in mainland China (1 vs. 1/6) during SON is significantly different at the 5% level between warm and cold TNA SST years. This is consistent with the significant positive correlation between MAM TNA SSTA and SON frequency of intense TC landfalls in mainland China.

Track map of intense TCs landfalling in mainland China during SON of selected warm and cold TNA SST years (Figure 4) indicates that all of intense TCs landfalling in mainland China take northwestward tracks. Compared with cold TNA SST years, the larger number of intense TCs landfalling in mainland China during warm TNA SST years generate over the WWNP (10° – 20° N, 130° – 145° E), which corresponds to the area with higher genesis frequency of intense TCs (Figure 3c) and higher genesis frequency of all TCs (Gao *et al.*, 2018a, their Figure 3c). Rapid/slow intensification events of these intense TCs mainly occur in the region (10° – 25° N, 125° – 145° E), which is called key development region. Large-scale environmental conditions possibly

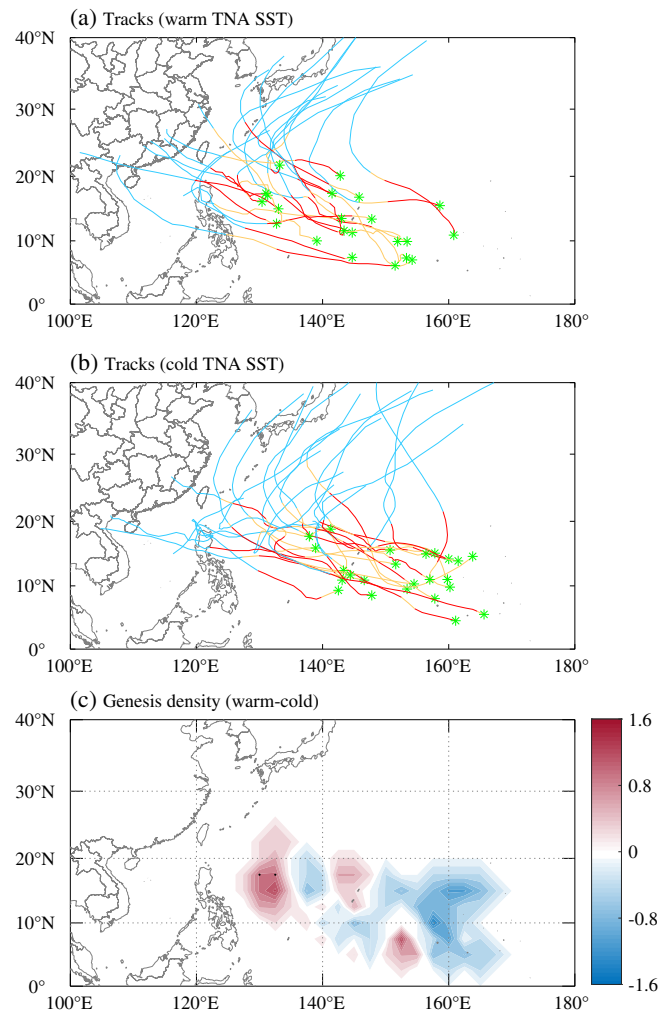


FIGURE 3 Tracks of all intense TCs during SON of (a) warm and (b) cold TNA SST years and (c) their difference in genesis density. In (a) and (b), green asterisks denote the genesis locations of intense TCs; orange, red, and blue tracks represent slow intensification events ($0 \text{ kt} < \Delta V_{24} < 30 \text{ kt}$), rapid intensification events ($\Delta V_{24} \geq 30 \text{ kt}$), and decay events ($\Delta V_{24} \leq 0 \text{ kt}$), respectively. In (c), values above the 95% confidence level are stippled

related to TC genesis and intensification are then examined. Figure 5 shows the composite differences in 850-hPa relative vorticity, 600-hPa relative humidity, maximum potential intensity (MPI, which is in close association with SST; Emanuel, 1988), and 200–850-hPa vertical wind shear between SON of warm and cold TNA SST years. Significantly higher MPI (Figure 5c) is observed over the WWNP during warm TNA SST years, suggesting its crucial role in the genesis and intensification of intense TCs landfalling in China. However, low-level relative vorticity (Figure 5a) and vertical wind shear (Figure 5d) are responsible for the genesis of a larger number of intense TCs over the southeastern WNP during cold TNA SST years.

Figure 6 indicates the composite difference in steering flow (i.e., 500-hPa wind field) between SON of warm and cold TNA SST years. The mean locations of WNP

subtropical high shown as 5,880-gpm contours are nearly identical during SON of warm and cold TNA SST years, and the associated steering flow surrounding those intense TCs landfalling in mainland China (Figure 4) shows no significant difference. It is widely accepted that TC landfalls are mainly determined by genesis location and steering flow (e.g., Liu and Chan, 2003; Goh and Chan, 2010; Zhang *et al.*, 2012a). The results therefore suggest that the higher frequency of intense TCs landfalling in mainland China during SON of warm TNA SST years is mainly attributed to the higher genesis frequency of intense TCs over the WWNP, they merely

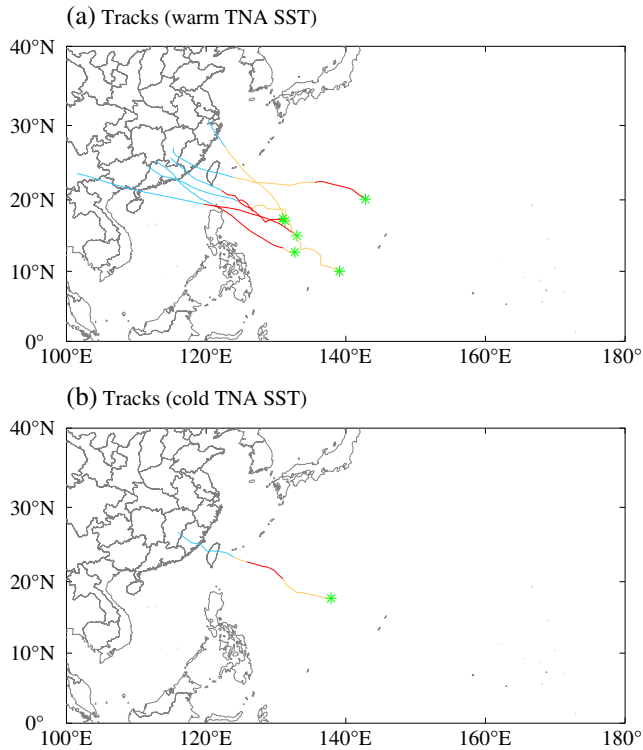


FIGURE 4 Same as Figure 3a,b, but for tracks of intense TCs landfalling in mainland China during SON

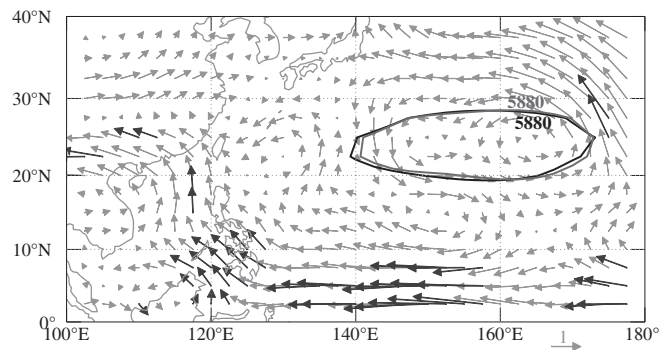


FIGURE 6 Difference in steering flow during SON of warm and cold TNA SST years. Black vectors denote values above the 95% confidence level. The red/blue 5,880-gpm contours denote the mean locations of subtropical high during SON of warm/cold TNA SST years

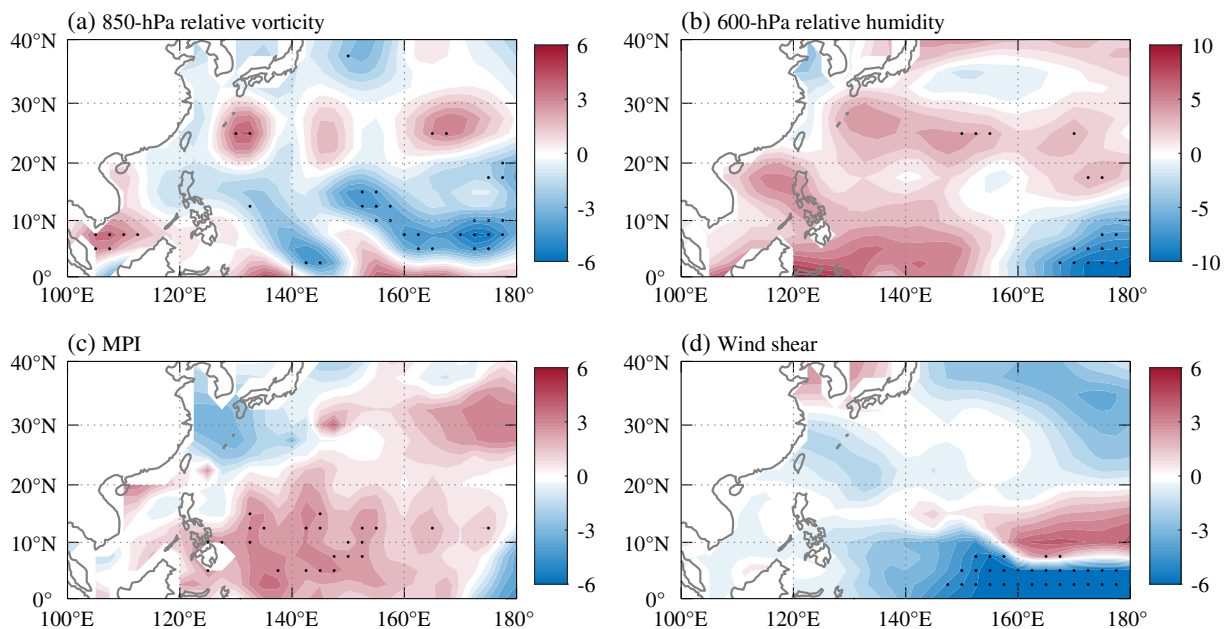


FIGURE 5 Differences in (a) 850-hPa relative vorticity (10^{-6} s^{-1}), (b) 600-hPa relative humidity (%), (c) MPI ($\text{m} \cdot \text{s}^{-1}$), and (d) vertical wind shear ($\text{m} \cdot \text{s}^{-1}$) during SON of warm and cold TNA SST years. Values above the 95% confidence level are stippled

follow the climatologically mean southeasterly steering flow and make landfall in mainland China. This is consistent with Gao *et al.* (2018b) who showed an important role of genesis location/frequency anomalies and a minor role of steering flow anomalies in regulating TC landfalls in East Asia during anomalous TNA SST years.

Possible mechanisms of the impact of MAM TNA SSTA on large-scale circulation over the WNP in the following SON are illustrated in Figure 7, which shows the regressions of SST, 850-hPa wind, and precipitation during MAM, June to August (JJA), and SON onto MAM TNA SSTA based on observation data, after removing the linear effects of ENSO in preceding DJF. Climatologically mean 850-hPa winds in three seasons during 1979–2017 are shown in Figure 8. During MAM (Figures 7a and 8a), a warm TNA SSTA in MAM induces anomalous low-level cyclonic flow over the subtropical eastern North Pacific as a Gill-type Rossby wave response (Gill, 1980). Northerly anomalies on the west flank of this anomalous cyclonic flow give rise to subtropical surface cooling through the wind-evaporation-SST feedback (Xie and Philander, 1994) and therefore suppress precipitation. During JJA (Figures 7b and 8b), the negative precipitation anomaly over the off-equatorial eastern North Pacific generates low-level anticyclonic flow anomaly and thus enhances northerly anomalies on its east flank, which reinforces surface cooling and the negative precipitation anomaly. The strongly coupled processes among

the anomalies of negative SST, negative precipitation, and northerly flow result in a westward extension of the negative precipitation anomaly and the anomalous anticyclonic flow, and the impacts of TNA SSTA are therefore relayed to the western Pacific. The easterly anomalies associated with the anomalous subtropical anticyclonic flow trigger the equatorial central Pacific cooling through the wind-evaporation-SST feedback. During SON (Figures 7c and 8c), the equatorial central Pacific cooling is amplified and the equatorial easterlies are boosted through the Bjerknes feedback (Bjerknes, 1969). The SST warming in the WWNP arises due to the anomalous westward advection of warm surface water by the equatorial easterly anomalies. A La Niña-like condition during SON, which is plausibly forced by the warm TNA SSTA during MAM, has therefore developed. This is generally consistent with the findings by Ham *et al.* (2013a, 2013b) and Cai *et al.* (2019).

To verify the modulation of MAM TNA SSTA on large-scale circulation in the Pacific, we perform the CTRL and TNA experiments using the CESM (see Section 2). The ensemble-mean differences in 850-hPa wind and SST between the two experiments (TNA minus CTRL) are shown in Figure 9. The forced responses to MAM TNA SSTA during three seasons strongly resemble to the regressed patterns onto MAM TNA SSTA based on observations (Figure 7), although the northerly anomalies over the subtropical eastern North Pacific during MAM (Figure 9a)

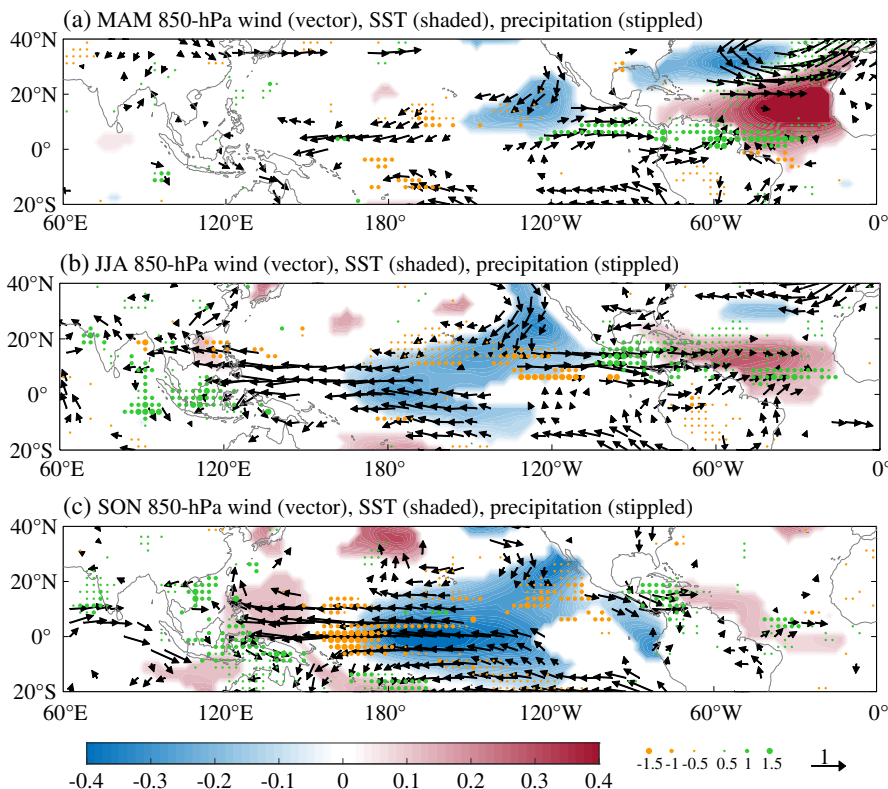


FIGURE 7 Regressions of SST (shaded, °C), 850-hPa wind field (vector, $\text{m}\cdot\text{s}^{-1}$), and precipitation (stippled, $\text{mm}\cdot\text{h}^{-1}$) anomalies during (a) MAM, (b) JJA, and (c) SON onto MAM TNA SSTA after removing the effects of ENSO in preceding DJF. Only the regression coefficients above the 95% confidence level are shown

FIGURE 8 Climatologically mean 850-hPa wind in (a) MAM, (b) JJA, and (c) SON during the period 1979–2017

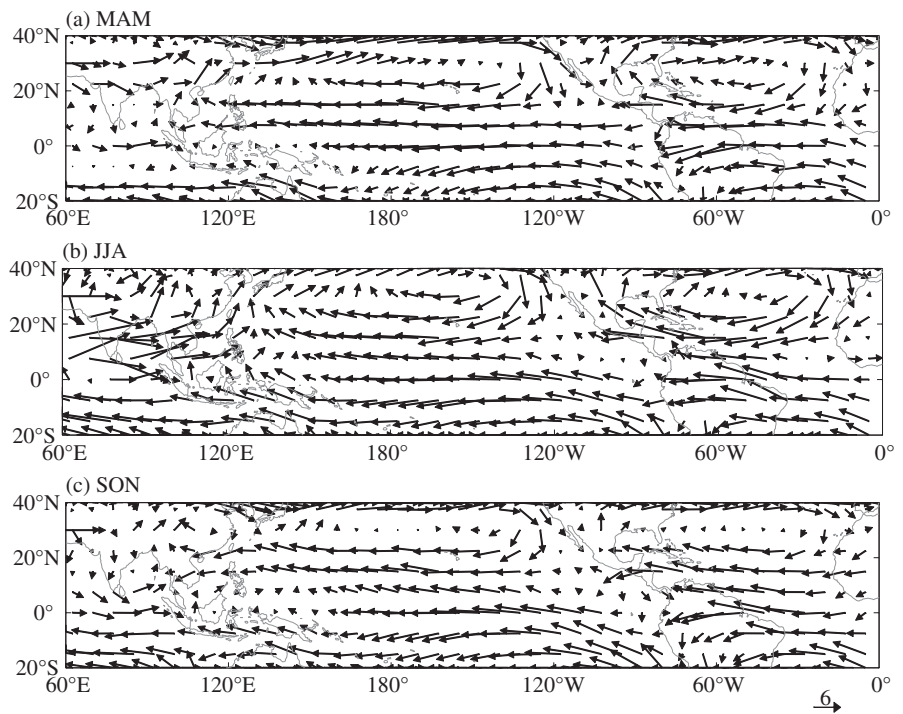
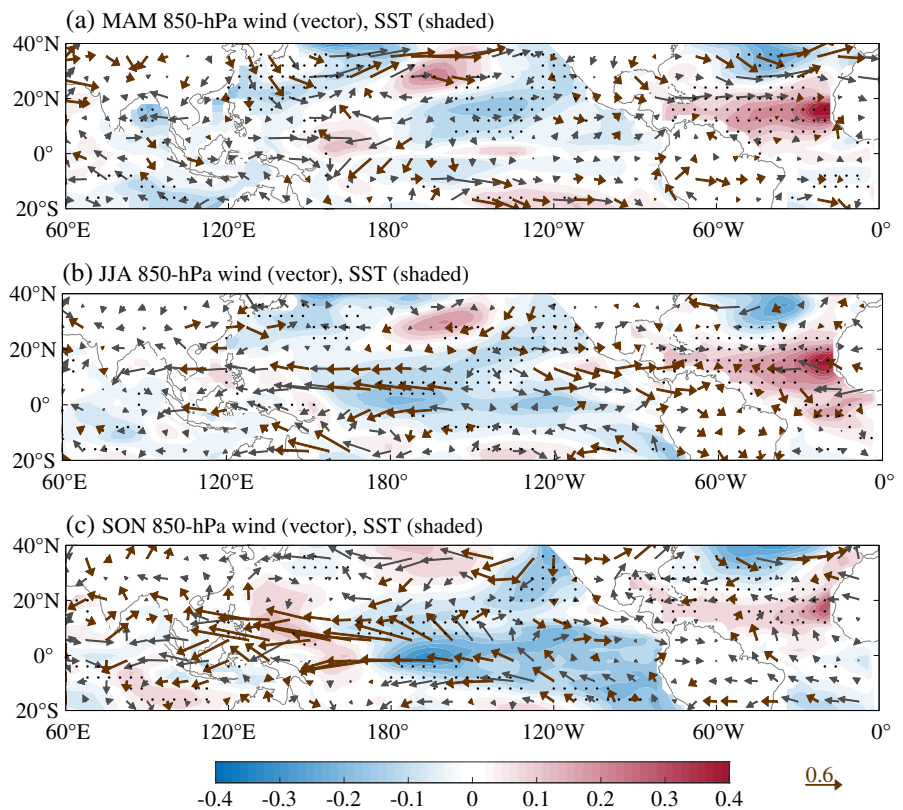


FIGURE 9 The ensemble-mean differences in 850-hPa wind field (vector, $\text{m}\cdot\text{s}^{-1}$) and SST (shaded, $^{\circ}\text{C}$) during (a) MAM, (b) JJA, and (c) SON between the TNA and CTRL experiments (TNA minus CTRL). Brown vectors and stippled areas show winds and SST above the 95% confidence level, respectively



are slightly weaker than observations (Figure 7a). This confirms that the warm TNA SSTA during MAM can trigger the warm WWNP SSTA (i.e., a La Niña-like condition)

during SON, the associated higher MPI (Figure 5c) is favourable for the genesis and intensification of those intense TCs landfalling in mainland China.

4 | SUMMARY AND DISCUSSION

Different from the significant negative relationship of WNP TC frequency and landfalling TC frequency with TNA SST reported in previous studies (Huo *et al.*, 2015; Cao *et al.*, 2016; Yu *et al.*, 2016; Zhang *et al.*, 2017; Gao *et al.*, 2018a), we have found a significant positive correlation between TNA SST during preceding MAM and frequency of intense TCs landfalling in mainland China during SON. Based on the observational analyses, we have examined the impacts of MAM TNA SSTA on SON large-scale circulation over the WNP after minimizing the ENSO effects. Through a chain of Gill-type Rossby wave response, wind-evaporation-SST feedback, and warm water advection, a warm TNA SSTA during MAM can induce a warm SSTA in the WWNP (i.e., a La Niña-like condition) during subsequent SON. Such physical mechanisms are well reproduced by a suite of coupled experiments with the state-of-the-art NCAR CESM. The warmer SST (i.e., the higher MPI) is favourable for the genesis of intense TCs over the WWNP and their subsequent intensification, and those intense TCs tend to make landfall in mainland China by following the climatological mean steering flow. The sign differences between the correlations of TC genesis frequency over the entire WNP and over the WWNP with the same TNA SST forcing can be attributed to different environmental factors responsible for TC genesis in different subregions of the WNP. In other words, it is the higher MPI that leads to more TC geneses over the WWNP during warm TNA SSTA years, and it is the larger vorticity, the weaker vertical shear and/or the higher mid-level humidity that result in more TC geneses over the other regions of WNP during cold TNA SSTA years.

Our findings pave the way for seasonal forecasts of intense TCs landfalling over the Chinese coast with high population density and booming infrastructures. The SSTA in the TNA during spring can be used as a physically-based predictor for next-season intense TC landfalls in China. Given the increasing trend in TNA SST (e.g., Knutson *et al.*, 2010), we also perform the observational analyses using the original data and find similar results, suggesting that TNA SST may influence large-scale circulation and therefore intense TC activity over the WNP on time scales longer than the interannual periodicity reported here. This is worthy to be further explored in future studies.

ACKNOWLEDGEMENTS

We thank the editor and anonymous reviewers for insightful comments that improve the quality of this paper. NCEP/NCAR reanalysis data, GPCP V2.3 precipitation data and NOAA ERSST V4 data are provided by the NOAA/OAR/ESRL PSD, Boulder, Colorado, USA,

from their website at <https://www.esrl.noaa.gov/psd/>. TC best track data set is provided by the JTWC at <http://www.metoc.navy.mil/jtwc/jtwc.html?best-tracks>. CESM codes are provided by the NCAR at <http://www.cesm.ucar.edu/>. This study was supported by the National Key R&D Program of China (Grant No. 2019YFC1510400), the National Natural Science Foundation of China (Grant Nos. 41930967, 41575078, 41975054) and the Strategic Priority Research Program of the Chinese Academy of Sciences (Grant No. XDA20100304).

ORCID

Wei Zhang  <https://orcid.org/0000-0001-8134-6908>

REFERENCES

- Adler, R.F., Sapiano, M., Huffman, G.J., Wang, J.-J., Gu, G., Bolvin, D., et al. (2018) The global precipitation climatology project (GPCP) monthly analysis (new version 2.3) and a review of 2017 global precipitation. *Atmosphere*, 9(4), 138. <https://doi.org/10.3390/atmos9040138>.
- Bjerknes, J. (1969) Atmospheric teleconnections from the equatorial Pacific. *Monthly Weather Review*, 97(3), 163–172. [https://doi.org/10.1175/1520-0493\(1969\)097<0163:ATFTEP>2.3.CO;2](https://doi.org/10.1175/1520-0493(1969)097<0163:ATFTEP>2.3.CO;2).
- Cai, W., Wu, L., Lengaigne, M., Li, T., McGregor, S., Kug, J.-S., Yu, J.Y., Stuecker, M.F., Santoso, A., Li, X., Ham, Y.G., Chikamoto, Y., Ng, B., McPhaden, M.J., du, Y., Dommenges, D., Jia, F., Kajtar, J.B., Keenlyside, N., Lin, X., Luo, J.J., Martín-Rey, M., Ruprich-Robert, Y., Wang, G., Xie, S. P., Yang, Y., Kang, S.M., Choi, J.Y., Gan, B., Kim, G.I., Kim, C. E., Kim, S., Kim, J.H. and Chang, P. (2019) Pantropical climate interactions. *Science*, 363(6430), eaav4236. <https://doi.org/10.1126/science.aav4236>.
- Cao, X., Chen, S., Chen, G. and Wu, R. (2016) Intensified impact of northern tropical Atlantic SST on tropical cyclogenesis frequency over the western North Pacific after the late 1980s. *Advances in Atmospheric Sciences*, 33(8), 919–930. <https://doi.org/10.1007/s00376-016-5206-z>.
- Chan, J.C.L. (2007) Interannual variations of intense typhoon activity. *Tellus A: Dynamic Meteorology and Oceanography*, 59(4), 455–460. <https://doi.org/10.1111/j.1600-0870.2007.00241.x>.
- Chan, J.C.L. (2008) Decadal variations of intense typhoon occurrence in the western North Pacific. *Proceedings of the Royal Society A: Mathematical, Physical and Engineering Sciences*, 464 (2089), 249–272. <https://doi.org/10.1098/rspa.2007.0183>.
- Chen, D., Zebiak, S.E., Busalacchi, A.J. and Cane, M.A. (1995) An improved procedure for El Niño forecasting: implications for predictability. *Science*, 269(5231), 1699–1702. <https://doi.org/10.1126/science.269.5231.1699>.
- Elsner, J.B. and Liu, K.-B. (2003) Examining the ENSO-typhoon hypothesis. *Climate Research*, 25(1), 43–54. <https://doi.org/10.3354/cr025043>.
- Emanuel, K.A. (1988) The maximum intensity of hurricanes. *Journal of the Atmospheric Sciences*, 45(7), 1143–1155. [https://doi.org/10.1175/1520-0469\(1988\)045<1143:TMIOH>2.0.CO;2](https://doi.org/10.1175/1520-0469(1988)045<1143:TMIOH>2.0.CO;2).
- Fogarty, E.A., Elsner, J.B., Jagger, T.H., Liu, K.B. and Louie, K.S. (2006) Variations in typhoon landfalls over China. *Advances in*

- Atmospheric Sciences*, 23(5), 665–677. <https://doi.org/10.1007/s00376-006-0665-2>.
- Gao, S., Zhai, S., Chiu, L.S. and Xia, D. (2016) Satellite air-sea enthalpy flux and intensity change of tropical cyclones over the western North Pacific. *Journal of Applied Meteorology and Climatology*, 55(2), 425–444. <https://doi.org/10.1175/JAMC-D-15-0171.1>.
- Gao, S., Zhai, S., Chen, B. and Li, T. (2017) Water budget and intensity change of tropical cyclones over the western North Pacific. *Monthly Weather Review*, 145(8), 3009–3023. <https://doi.org/10.1175/MWR-D-17-0033.1>.
- Gao, S., Chen, Z. and Zhang, W. (2018a) Impacts of tropical North Atlantic SST on western North Pacific landfalling tropical cyclones. *Journal of Climate*, 31(2), 853–862. <https://doi.org/10.1175/JCLI-D-17-0325.1>.
- Gao, S., Zhu, L., Zhang, W. and Chen, Z. (2018b) Strong modulation of the Pacific meridional mode on the occurrence of intense tropical cyclones over the western North Pacific. *Journal of Climate*, 31(19), 7739–4479. <https://doi.org/10.1175/JCLI-D-17-0833.1>.
- Gao, S., Zhu, L., Zhang, W. and Shen, X. (2020) Impact of the Pacific meridional mode on landfalling tropical cyclone frequency in China. *Quarterly Journal of the Royal Meteorological Society*, 1–11. <https://doi.org/10.1002/qj.3799>.
- Gill, A.E. (1980) Some simple solutions for heat-induced tropical circulation. *Quarterly Journal of the Royal Meteorological Society*, 106(449), 447–462. <https://doi.org/10.1002/qj.49710644905>.
- Goh, A.Z.C. & Chan, J.C.L. (2010) An improved statistical scheme for the prediction of tropical cyclones making landfall in south China. *Weather and Forecasting*, 25(2), 587–593. <https://doi.org/10.1175/2009WAF2222305.1>.
- Ham, Y.-G., Kug, J.-S. and Park, J.-Y. (2013a) Two distinct roles of Atlantic SSTs in ENSO variability: north tropical Atlantic SST and Atlantic Niño. *Geophysical Research Letters*, 40(15), 4012–4017. <https://doi.org/10.1002/grl.50729>.
- Ham, Y.-G., Kug, J.-S., Park, J.-Y. and Jin, F.-F. (2013b) Sea surface temperature in the north tropical Atlantic as a trigger for El Niño/southern oscillation events. *Nature Geoscience*, 6, 112–116. <https://doi.org/10.1038/ngeo1686>.
- Huang, B., Banzon, V.F., Freeman, E., Lawrimore, J., Liu, W., Peterson, T.C., Smith, T.M., Thorne, P.W., Woodruff, S.D. and Zhang, H.M. (2015) Extended Reconstructed Sea surface temperature version 4 (ERSST.v4). Part I: upgrades and intercomparison. *Journal of Climate*, 28(3), 911–930. <https://doi.org/10.1175/JCLI-D-14-00006.1>.
- Huo, L., Guo, P., Hameed, S.N. and Jin, D. (2015) The role of tropical Atlantic SST anomalies in modulating western North Pacific tropical cyclone genesis. *Geophysical Research Letters*, 42(7), 2378–2384. <https://doi.org/10.1002/2015GL063184>.
- Hurrell, J.W., Holland, M.M., Gent, P.R., Ghan, S., Kay, J.E. and Kushner, P.J. (2013) The community earth system model: a framework for collaborative research. *Bulletin of the American Meteorological Society*, 94(9), 1339–1360. <https://doi.org/10.1175/BAMS-D-12-00121.1>.
- Kalnay, E., Kanamitsu, M., Kistler, R., Collins, W., Deaven, D., Gandin, L., Iredell, M., Saha, S., White, G., Woollen, J., Zhu, Y., Leetmaa, A., Reynolds, R., Chelliah, M., Ebisuzaki, W., Higgins, W., Janowiak, J., Mo, K.C., Ropelewski, C., Wang, J., Jenne, R. and Joseph, D. (1996) The NCEP/NCAR 40-year reanalysis project. *Bulletin of the American Meteorological Society*, 77(3), 437–471. [https://doi.org/10.1175/1520-0477\(1996\)077<0437:TNYRP>2.0.CO;2](https://doi.org/10.1175/1520-0477(1996)077<0437:TNYRP>2.0.CO;2).
- Knutson, T.R., McBride, J.L., Chan, J., Emanuel, K., Holland, G., Landsea, C., Held, I., Kossin, J.P., Srivastava, A.K. and Sugi, M. (2010) Tropical cyclones and climate change. *Nature Geoscience*, 3, 157–163. <https://doi.org/10.1038/ngeo779>.
- Li, R.C.Y., Zhou, W., Shun, C.M. and Lee, T.C. (2017) Change in destructiveness of landfalling tropical cyclones over China in recent decades. *Journal of Climate*, 30(9), 3367–3379. <https://doi.org/10.1175/JCLI-D-16-0258.1>.
- Liu, K.S. and Chan, J.C.L. (2003) Climatological characteristics and seasonal forecasting of tropical cyclones making landfall along the South China coast. *Monthly Weather Review*, 131, 1650–1662. <https://doi.org/10.1175//2554.1>.
- Liu, K.S. and Chan, J.C.L. (2018) Changing relationship between La Niña and tropical cyclone landfalling activity in South China. *International Journal of Climatology*, 38(3), 1270–1284. <https://doi.org/10.1002/joc.5242>.
- Lok, C.C.F. and Chan, J.C.L. (2017) Changes of tropical cyclone landfalls in South China throughout the twenty-first century. *Climate Dynamics*, 51(7–8), 2467–2483. <https://doi.org/10.1007/s00382-017-4023-0>.
- Mei, W. and Xie, S.-P. (2016) Intensification of landfalling typhoons over the Northwest Pacific since the late 1970s. *Nature Geoscience*, 9(10), 735–757. <https://doi.org/10.1038/ngeo2792>.
- Mendelsohn, R., Emanuel, K., Chonabayashi, S. and Bakkensen, L. (2012) The impact of climate change on global tropical cyclone damage. *Nature Climate Change*, 2(3), 205–209. <https://doi.org/10.1038/nclimate1357>.
- Park, D.-S.R., Ho, C.-H. and Kim, J.-H. (2014) Growing threat of intense tropical cyclones to East Asia over the period 1977–2010. *Environmental Research Letters*, 9(1), 014008. <https://doi.org/10.1088/1748-9326/9/1/014008>.
- Tu, J.-Y., Chou, C. and Chu, P.-S. (2009) The abrupt shift of typhoon activity in the vicinity of Taiwan and its association with western North Pacific–east Asian climate change. *Journal of Climate*, 22(13), 3617–3628. <https://doi.org/10.1175/2009JCLI2411.1>.
- Wang, L. and Chen, G. (2018a) Impact of the spring SST gradient between the tropical Indian Ocean and western Pacific on landfalling tropical cyclone frequency in China. *Advances in Atmospheric Sciences*, 35(6), 682–688. <https://doi.org/10.1007/s00376-017-7078-2>.
- Wang, L. and Chen, G. (2018b) Relationship between South China Sea summer monsoon onset and landfalling tropical cyclone frequency in China. *International Journal of Climatology*, 38(7), 3209–3214. <https://doi.org/10.1002/joc.5485>.
- Wu, L., Wang, B. and Geng, S. (2005) Growing typhoon influence on East Asia. *Geophysical Research Letters*, 32(18), L18703. <https://doi.org/10.1029/2005GL022937>.
- Wu, L. and Zhao, H. (2012) Dynamically-derived tropical cyclone intensity changes over the western North Pacific. *Journal of Climate*, 25(1), 89–98. <https://doi.org/10.1175/2011JCLI4139.1>.
- Wu, M.C., Chang, W.L. and Leung, W.M. (2004) Impacts of El Niño–southern oscillation events on tropical cyclone landfalling activity in the western North Pacific. *Journal of Climate*, 17(6), 1419–1428. [https://doi.org/10.1175/1520-0442\(2004\)017<1419:IOENOE>2.0.CO;2](https://doi.org/10.1175/1520-0442(2004)017<1419:IOENOE>2.0.CO;2).

- Xie, S.-P. and Philander, S.G.H. (1994) A coupled ocean-atmosphere model of relevance to the ITCZ in the eastern Pacific. *Tellus A: Dynamic Meteorology and Oceanography*, 46(4), 340–350. <https://doi.org/10.3402/tellusa.v46i4.15484>.
- Yu, J., Li, T., Tan, Z. and Zhu, Z. (2016) Effects of tropical North Atlantic SST on tropical cyclone genesis in the western North Pacific. *Climate Dynamics*, 46(3–4), 865–877. <https://doi.org/10.1007/s00382-015-2618-x>.
- Zhang, C., Hu, C., Huang, G., Yao, C., Zheng, Z., Wang, T., Wu, Z., Yang, S. and Chen, D. (2019) Perspective on landfalling frequency and genesis location variations of southern China typhoon during peak summer. *Geophysical Research Letters*, 46, 6830–6838. <https://doi.org/10.1029/2019GL083420>.
- Zhang, Q., Wu, L. and Liu, Q. (2009) Tropical cyclone damages in China 1983–2006. *Bulletin of the American Meteorological Society*, 90(4), 489–495. <https://doi.org/10.1175/2008BAMS2631.1>.
- Zhang, Q., Zhang, W., Lu, X. and Chen, Y.D. (2012b) Landfalling tropical cyclones activities in the South China: intensifying or weakening? *International Journal of Climatology*, 32(12), 1815–1824. <https://doi.org/10.1002/joc.2396>.
- Zhang, W., Graf, H.F., Leung, Y. and Herzog, M. (2012a) Different El Niño types and tropical cyclone landfall in East Asia. *Journal of Climate*, 25(19), 6510–6523. <https://doi.org/10.1175/JCLI-D-11-00488.1>.
- Zhang, W., Leung, Y. and Fraedrich, K. (2015) Different El Niño types and intense typhoons in the western North Pacific. *Climate Dynamics*, 44(11–12), 2965–2977. <https://doi.org/10.1007/s00382-014-2446-4>.
- Zhang, W., Vecchi, G.A., Murakami, H., Delworth, T., Wittenberg, A.T., Rosati, A., Underwood, S., Anderson, W., Harris, L., Gudgel, R., Lin, S.J., Villarini, G. and Chen, J.H. (2016) Improved simulation of tropical cyclone responses to ENSO in the western North Pacific in the high-resolution GFDL HiFLOR coupled climate model. *Journal of Climate*, 29(4), 1391–1415. <https://doi.org/10.1175/jcli-d-15-0475.1>.
- Zhang, W., Vecchi, G.A., Murakami, H., Villarini, G., Delworth, T. L., Yang, X. and Jia, L. (2018b) Dominant role of Atlantic multidecadal oscillation in the recent decadal changes in western North Pacific tropical cyclone activity. *Geophysical Research Letters*, 45(1), 354–362. <https://doi.org/10.1002/2017GL076397>.
- Zhang, W., Vecchi, G.A., Villarini, G., Murakami, H., Rosati, A., Yang, X., Jia, L. and Zeng, F. (2017) Modulation of western North Pacific tropical cyclone activity by the Atlantic meridional mode. *Climate Dynamics*, 48(1–2), 631–647. <https://doi.org/10.1007/s00382-016-3099-2>.
- Zhang, W., Villarini, G., Vecchi, G.A. and Smith, J.A. (2018a) Urbanization exacerbated the rainfall and flooding caused by hurricane Harvey in Houston. *Nature*, 563(7731), 384–388. <https://doi.org/10.1038/s41586-018-0676-z>.

How to cite this article: Gao S, Chen Z, Zhang W, Shen X. Effects of tropical North Atlantic sea surface temperature on intense tropical cyclones landfalling in China. *Int J Climatol*. 2020;1–10. <https://doi.org/10.1002/joc.6732>